Biophysical Journal
Article

Biophysical Society

pH-triggered pore-forming peptides with strong composition-dependent membrane selectivity

Sarah Y. Kim,[1] Ana-Nicoleta Bondar,[2,*] William C. Wimley,[3,*] and Kalina Hristova[1,*]
[1]Department of Materials Science and Engineering, Institute for NanoBioTechnology, and Program in Molecular Biophysics, Johns Hopkins University, Baltimore, Maryland; [2]Freie Universität Berlin, Department of Physics, Theoretical Molecular Biophysics Group, Berlin, Germany; and [3]Department of Biochemistry and Molecular Biology, Tulane University School of Medicine, New Orleans, Louisiana

ABSTRACT Peptides that self-assemble into nanometer-sized pores in lipid bilayers could have utility in a variety of biotechnological and clinical applications if we can understand their physical chemical properties and learn to control their membrane selectivity. To empower such control, we have used synthetic molecular evolution to identify the pH-dependent delivery peptides, a family of peptides that assemble into macromolecule-sized pores in membranes at low peptide concentration but only at pH $< \sim$6. Further advancements will also require better selectivity for specific membranes. Here, we determine the effect of anionic headgroups and bilayer thickness on the mechanism of action of the pH-dependent delivery peptides by measuring binding, secondary structure, and macromolecular poration. The peptide pHD15 partitions and folds equally well into zwitterionic and anionic membranes but is less potent at pore formation in phosphatidylserine-containing membranes. The peptide also binds and folds similarly in membranes of various thicknesses, but its ability to release macromolecules changes dramatically. It causes potent macromolecular poration in vesicles made from phosphatidylcholine with 14 carbon acyl chains, but macromolecular poration decreases sharply with increasing bilayer thickness and does not occur at any peptide concentration in fluid bilayers made from phosphatidylcholine lipids with 20-carbon acyl chains. The effects of headgroup and bilayer thickness on macromolecular poration cannot be accounted for by the amount of peptide bound but instead reflect an inherent selectivity of the peptide for inserting into the membrane-spanning pore state. Molecular dynamics simulations suggest that the effect of thickness is due to hydrophobic match/mismatch between the membrane-spanning peptide and the bilayer hydrocarbon. This remarkable degree of selectivity based on headgroup and especially bilayer thickness is unusual and suggests ways that pore-forming peptides with exquisite selectivity for specific membranes can be designed or evolved.

SIGNIFICANCE This article establishes the intricate and unique membrane selectivity of synthetically evolved peptides that self-assemble into nanometer-size pores in response to pH. The work has broad implications for the engineering of self-assembling peptide nanopores for a multitude of applications in biotechnology and medicine.

INTRODUCTION

Peptides that permeabilize membranes have many potential applications, including antiviral, antifungal, antibacterial, and anticancer applications (1–4). They can also be used in drug delivery applications to deliver cargos by transiently permeabilizing the plasma membrane or by permeabilizing endosomal membranes after the uptake of peptide and cargo (5–8). The biggest challenge in advancing membrane-permeabilizing peptides is the need to control membrane selectivity. Toward this goal of controlled membrane activity, we recently evolved a family of pH-sensitive, pore-forming peptides that release macromolecules from synthetic bilayers at very low concentrations but only at an acidic pH (9). These so-called "pH-dependent delivery (pHD) peptides" are inactive random coils in buffer at pH 7 and above. But when the pH is decreased below $\sim$6, they partition into synthetic lipid vesicles and simultaneously fold into α-helical secondary structure (9,10). When the number of bound peptides reaches an unusually low threshold of $\sim$1 peptide per 1000 lipids or $\sim$100 peptides per vesicle, the pHD peptides assemble into macromolecule-sized pores with radii between 3 and 10 nm (10) and release the vesicle contents.

Submitted September 9, 2020, and accepted for publication January 4, 2021.

*Correspondence: nbondar@zedat.fu-berlin.de or wwimley@tulane.edu or kh@jhu.edu

Editor: Roland Winter.

https://doi.org/10.1016/j.bpj.2021.01.010

To date, the pH-triggered activity of the pHD peptides has been described only for synthetic bilayers made from zwitterionic 1-palmitoyl-2-oleoyl-*sn*-glycero-3-phosphocholine (POPC) or C16:0,C18:1(9)-PC. POPC is a very widely used mimic of the generic physical chemical properties of fluid-phase mammalian plasma membranes. However, for maximal utility, pore-forming peptides must be tuned to selectively act upon particular biological membranes, which are composed of hundreds of different lipid species with different headgroups, zwitterionic or anionic, and various acyl chains that affect the physical properties of the membrane (11–15). These properties can control the activity of peptides. In particular, membrane charge and thickness have been shown to modulate the binding, aggregation, and activity of peptides (16–31). Here, we seek to understand how these important aspects of lipid composition affect the macromolecular poration activity of the pHD peptides.

We test the effect of these two critical bilayer properties, headgroup charge and bilayer thickness, on the activity of pHD15 (sequence: GIGEVLHELADDLPDLQEWIHAA QQL-amide). We find that pHD15 generally retains its pH-sensitive binding and helical secondary structure in all bilayers tested. However, its insertion into the transmembrane pore state and macromolecular poration activity is sensitive to lipid composition, showing much less activity in 1-palmitoyl-2-oleoyl-*sn*-glycero-3-phospho-L-serine (POPS)-containing bilayers compared to POPC only. Most remarkably, pHD15 activity is highly sensitive to bilayer thickness. The peptide has very potent activity in fluid PC bilayers made from lipids with 14-carbon acyl chains yet is functionally inactive in fluid-phase bilayers made from PC lipids with 20-carbon acyl chains, despite similar, strong pH-dependent binding and α-helix formation in both PC bilayers. The exquisite sensitivity of macromolecular poration to bilayer properties arises from the physical chemistry of insertion into the transmembrane pore state from the interfacially bound state. Understanding this sensitivity will be an important step toward the design of membrane-selective pore-forming peptides.

MATERIALS AND METHODS

Peptides of >95% purity were purchased from Bio-Synthesis (Lewisville, TX). The lipids 1-palmitoyl-2-oleoyl-*sn*-glycero-3-phosphocholine (POPC), 1-palmitoyl-2-oleoyl-*sn*-glycero-3-phosphoserine (POPS), 1-palmitoyl-2-oleoyl-*sn*-glycero-3-phospho-(1′-rac-glycerol) (POPG), 1,2-dimyristoleoyl-*sn*-glycero-3-phosphocholine (C14PC), 1,2-dipalmitoleoyl-*sn*-glycero-3-phosphocholine (C16PC), 1,2-dioleoyl-*sn*-glycero-3-phosphocholine (C18PC), 1,2-dieicosenoyl-*sn*-glycero-3-phosphocholine (C20PC), and 1,2-dierucoyl-*sn*-glycero-3-phosphocholine (C22PC) were purchased from Avanti Polar Lipids (Alabaster, AL). 8-Aminonaphthalene-1,2,3-trisulfonic acid and p-xylylenebis (pyridinium bromide) were purchased from Thermo Fisher Scientific (Waltham, MA). Chloroform, ammonium thiocyanate, and other salts and buffer materials were purchased from Thermo Fisher Scientific or Sigma-Aldrich (St. Louis, MO). Tetramethylrhodamine (TAMRA)-biotin-dextran (TBD) was synthesized as described elsewhere (9,32,33).

Buffers

Thirteen buffers were prepared with pH from 4 to 7 at 0.25 pH increments. Buffers with a pH between 4 and 5.5 were prepared with 10 mM sodium acetate, and buffers with a pH between 5.75 and 7 were prepared with 10 mM sodium phosphate. Buffers for binding and leakage assays were prepared with 100 mM KCl. Buffers for circular dichroism (CD) were prepared without KCl, and their pH was adjusted with phosphatidic acid instead of hydrochloric acid to avoid the absorption of the chloride ion below 200 nm. All buffers were vacuum filtered through a 0.22-μm pore size membrane to remove dust and bacteria before use.

Peptides

Solutions of ~1 mM pHD15 were prepared with Millipore water (MilliporeSigma, Burlington, MA). Concentrations were determined using the absorbance of the single tryptophan on the peptide. The average of three absorbance measurements at 280 nm on a NanoDrop 2000c (Thermo Fisher Scientific) was used to determine the concentration. Peptides were stored frozen until use and were subjected to no more than five freeze-thaws to minimize peptide degradation.

Vesicle preparation

Large unilamellar vesicles of ~100-nm diameter were prepared with the lipid compositions POPC, 1:9 POPS:POPC, 1:9 POPG:POPC, C14PC, C16PC, C18PC, C20PC, or C22PC. For all vesicle types, lipid dissolved in chloroform was dried under vacuum overnight, resuspended in buffer, and extruded 10 times through 100 nm Nucleopore polycarbonate membranes using a handheld syringe extruder made by Avanti Polar Lipids. Vesicles with no entrapped probes were used for binding and CD. For vesicles with encapsulated TBD, dry lipid films were resuspended in buffer containing 1 mg TBD per 50 μmol lipid. The samples were frozen and thawed 10 times before extrusion. After extrusion, vesicles were incubated on high-capacity streptavidin agarose to remove unencapsulated TBD. Lipid concentration was measured using a modified Stewart assay (34). Vesicle size and uniformity were evaluated by dynamic light scattering on a Zetasizer Nano (Nano Zetasizer; Malvern Instruments, Worcestershire, UK) to have an average size of 118 $\pm$ 7 nm and an average polydispersity index of 0.08 $\pm$ 0.02 (indicating low polydispersity). Vesicles were used either on the same day or stored at 4°C and used 1–3 days after their preparation.

Dextran leakage assays

Leakage of 40 kDa dextran from vesicles was measured using a Förster resonance energy transfer (FRET) assay (9,32,33). Dextran vesicles with entrapped TBD were diluted to 1 mM, and streptavidin-AlexaFluor488 (AF488) (the donor fluorophore) was added to a final concentration of 20 nM. In a 96-well plate, peptide and vesicles were mixed and then incubated while shaking at room temperature for 1 h before measuring FRET by donor fluorescence quenching on a BioTek H4 Synergy Hybrid Microplate Reader with excitation/emission = 495/519 nm (BioTek Instruments, Winooski, VT). As a positive control for 100% leakage, 4 μL of 10% Triton X-100 was added to three wells. As a negative control, no peptide was added to three wells. Leakage measurements are the average of at least three unique vesicle preparations. Fractional leakage was calculated as follows:

$$f_{leakage} = \left(F_{no\ peptide} - F_{sample}\right) \Big/ \left(F_{no\ peptide} - F_{Triton}\right). \quad (1)$$

The leakage as a function of pH was fit to determine the pH at which leakage is 50% (the midpoint or "pH_{50}"):

$$f_{leakage} = L_{max} + \frac{L_{min} - L_{max}}{1 + e^{\frac{pH50 - pH}{rate}}}. \quad (2)$$

Here, L_{max} and L_{min} are the curve's maximal and minimal values, respectively, and *rate* describes the steepness of the curve.

Tryptophan binding

Vesicles were prepared at ~30 mM at pH 4.75 and pH 6.25 as described above. Vesicles were diluted to 1 mM with buffers spanning pH 4–7 and then incubated overnight at 4°C to allow the internal and external pH to equilibrate while minimizing vesicle degradation due to hydrolysis. The next morning, the pH of the solution was verified with MColorpHast pH test strips (MilliporeSigma). Peptide was added with peptide-to-lipid ratio (P:L) ranging from 1:50 to 1:5000 in 0.5-mL centrifuge tubes. After 1 h of incubation at room temperature, tryptophan fluorescence spectra were measured on a HORIBA Fluorolog 3–22 (HORIBA, Kyoto, Japan) in a 45-μL cuvette. Polarizers were inserted into the light path oriented at 90° for the excitation light and 0° for the emission light to reduce the effect of light scattering (35). The fluorescence from 330 to 335 nm was averaged and normalized from 0 to 1. The midpoint of the curve, or the pH_{50}, was obtained by fitting using Eq. 2. The nmol of peptide bound was calculated as follows:

$$N_{bound} = f_{bound} N_{total}, \quad (3)$$

where f_{bound} is the fraction of peptide bound, as determined by the normalized tryptophan fluorescence, and N_{total} is the total nmol of peptide in a sample.

Circular dichroism

Vesicles without KCl were prepared as described above for tryptophan binding. Scans were collected in a 1-mm pathlength cuvette on a Jasco J-715 spectropolarimeter (JASCO, Easton, MD) with a scan rate of 100 nm/min, three accumulations, at room temperature. After measurement, the scans were corrected for background using a vesicle sample with no peptides. Relative percentage of helicity was calculated by scaling the average ellipticity at 217–227 nm. The midpoint of the curve, or the pH_{50}, was obtained by fitting using Eq. 2.

Oriented circular dichroism

Mixtures of peptide and lipid were prepared in methanol at P:L = 1:50 for pHD15. Aliquots were dried under vacuum onto a quartz disk for at least 1 h. The disk was sealed in a chamber with a second quartz window. The samples were allowed to hydrate for at least 30 min through the vapor phase using Milli-Q water (MilliporeSigma) in the chamber to form stacked oriented multibilayers. The quartz disk was oriented perpendicular to the beam, and CD spectra were collected at eight rotations of the sample holder around the beam axis and averaged. Lipid-only spectra, collected the same way, were subtracted.

Molecular dynamics simulation

Coordinates for the peptide in α-helical conformation were generated using Phyre2 (36,37). The peptide was then oriented with its principal axis along the membrane normal using Visual Molecular Dynamics, VMD (38). The peptide was positioned such that its center of mass was in the center of Cartesian coordinates using Chemistry at Harvard Molecular Mechanics (CHARMM) (39). All carboxylate groups were considered neutral, and the histidine groups were singly protonated on Nε2. We used CHARMM-GUI (40) to prepare three simulation systems with the peptide embedded in C14PC, POPC, and C20PC. Sodium ions were added to bulk water for charge neutrality. Hydrated lipid membranes contained 289–296 lipid molecules, for a total of 76,420–80,953 atoms.

Interactions between atoms of the system were described with CHARMM 36 (41–44) with TIP3P water (45). All simulations were performed with NAMD (46,47). Equilibration was performed with velocity rescaling and positional restraints as set by standard CHARMM-GUI, and with an integration timestep of 1 fs. All positional restraints were then switched off, and the simulation continued for 1 ns with 1-fs integration steps. For the remaining of the simulations, we used a multiple time integration step (48,49) of 1 fs for the bonded forces, 2 fs for short-range nonbonded forces, and 4 fs for long-range nonbonded forces. We used a switching function between 10 and 12 Å for the short-range real-space interactions and smooth particle mesh Ewald summation (50,51) for Coulomb interactions. Coordinates were saved each 10 ps. Average values were computed from the last 100 ns of each simulation.

RESULTS

The pHD peptides were evolved by screening an iterative, second-generation peptide library for a unique activity, macromolecular poration, in 1-palmitoyl-2-oleoyl-*sn*-glycero-3-phosphocholine (POPC) lipid vesicles at pH 7 and pH 5 (9). The selected pHD peptides are highly active only at pH 5 but not at pH 7. They have been extensively characterized in POPC bilayers in which they assemble into very large membrane-spanning pores (10). Although POPC is a widely used generic mimic of fluid phase, zwitterionic cell membranes, the engineering and optimization of pHD peptide activity, or the action of any membrane-active peptide requires a knowledge of how lipid headgroups, including headgroup charge, and bilayer thickness affect activity. For this work, we selected pHD15 and measured membrane binding, secondary structure, and macromolecular poration in bilayers with varied physical properties. First, we tested bilayers of POPC plus 10% of anionic lipids with the same chains: phosphatidylglycerol (POPG) or phosphatidylserine (POPS). These headgroups are highly relevant to potential applications as PS lipids are abundant in mammalian membranes including the plasma membrane (25), whereas PG lipids mimic abundant endosome-specific lipids with glycerol headgroups. Second, we also measured pHD15 activity in fluid-phase bilayers made from symmetric diacyl PC lipids with monounsaturated acyl chains ranging from 14 to 20 carbons to mimic bilayers of different biologically relevant thicknesses.

Macromolecular leakage across anionic membranes in response to pHD15

To evaluate the activity of pHD15, a FRET-based macromolecule leakage assay (9,32,33) was used (Fig. 1 *A*). The acceptor molecule, TAMRA- and biotin-labeled dextran 40 kDa (TBD), is encapsulated inside unilamellar lipid vesicles, and the donor molecule, AF488-labeled streptavidin, is added outside the vesicles. If the peptide creates

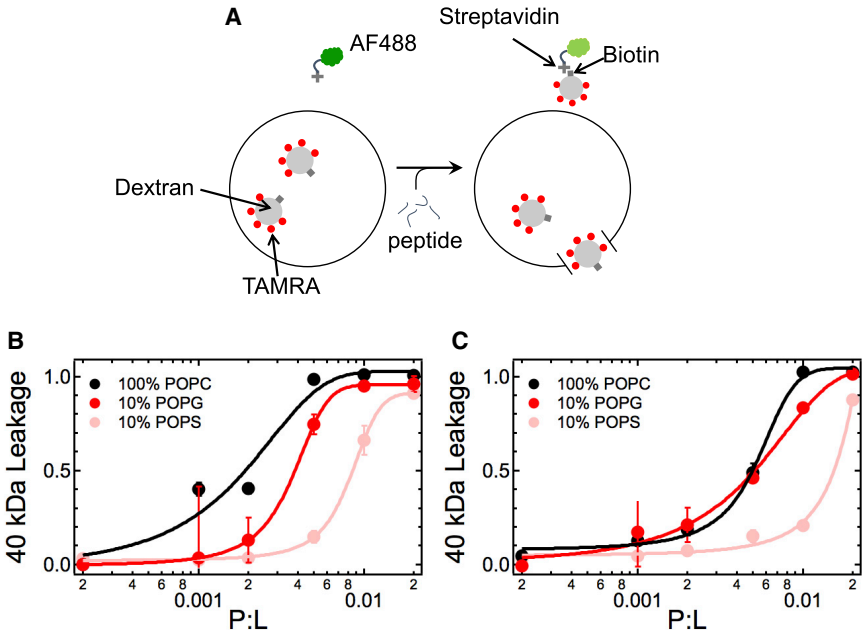

FIGURE 1 Macromolecular leakage across anionic membranes in response to pHD15. (*A*) Shown is a schematic of the FRET-based dextran leakage assay to measure the formation of large pores (*B* and *C*). Shown is leakage of 40 kDa dextran from vesicles composed of POPC, POPC + 10% POPG, and POPC + 10% POPS at pH 4.5 (*B*) and pH 5.5 (*C*). Peptide was incubated with 1 mM lipid for 1 h before FRET was measured. Data shown are the average of three replicates. Error bars represent standard deviations. To see this figure in color, go online.

macromolecule-sized pores in the vesicles, TBD is released and will form biotin-bridged complexes with streptavidin, resulting in quenching of AF488 fluorescence by TAMRA. The detergent Triton X-100 is a positive control for 100% leakage.

In Fig. 1, *B* and *C*, we show the fractional leakage of TBD, measured 1 h after the addition of the peptide as a function of P:L. Leakage was assessed at pH 4.5 (Fig. 1 *B*) and pH 5.5 (Fig. 1 *C*), both below the pH at which pore formation is triggered. At the lowest peptide concentrations, little or no leakage is observed at either pH, whereas at the higher peptide concentrations, 100% leakage is observed. We define leakage potency using LIC_{50}, the peptide-to-lipid ratio (P:L) ratio that causes 50% leakage. In POPC membranes, pHD15 has LIC_{50} of 1:520 at pH 4.5 and LIC_{50} of 1:185 at pH 5.5. In bilayers containing 10% phosphatidylserine (POPS), leakage activity is lower, with LIC_{50} of 1:120 and 1:65 at the two pH values. Leakage activity is affected less by the same surface charge when it is due to 10% phosphatidylglycerol (POPG).

To determine if the effects of headgroup on poration activity result from a shift in binding equilibria, we used tryptophan fluorescence titration (35) to measure the binding of pHD15 to the three types of vesicles. Peptide was incubated with increasing vesicle concentrations for 1 h, and tryptophan fluorescence spectra were measured. A shift in the emission spectrum to lower wavelengths and an increase in intensity results from membrane binding and insertion of the Trp residue into the less polar membrane environment (35). At low pH, pHD peptides are essentially completely bound (9,10) in all lipids. The wavelength of emission maximum was ~325 in all vesicle types, suggesting a similar environment of reduced polarity for the Trp residues of the bound peptides. The net intensity changes for complete binding were smaller in PG/PS vesicles compared to PC, but in Fig. 2 *B*, we normalized the fluorescence changes to enable comparison of the pH response in each vesicle type. There were no significant differences in binding to POPC or to POPC with 10% POPS or 10% POPG. Therefore, the differences in activity (Fig. 1) are not due to differences in binding. The fact that 10% anionic lipids does not affect binding of the pHD peptides suggests that their pH-sensitive activity occurs when they are roughly neutral.

To determine if the effects of headgroup on the activity of pHD15 are due to differences in folding into α-helical structure, which is essential for pHD activity (10), we collected circular dichroism (CD) spectra as functions of pH and P:L in POPC bilayers with and without 10% POPS. Example spectra in Fig. 3 *A* show a sharp random coil to α-helix transition as the pH is decreased, resulting in a low pH spectrum consistent with high helical content (10). Thus, α-helical structure formation mirrors binding. The normalized helicity at 222 nm is shown as a function of pH for three P:L ratios, P:L = 1:50, 1:100, and 1:200, in Fig. 3, *B–D*. The pH-dependent transitions of the pHD15 helical structure are very similar for POPC and POPC with 10% POPS. The pH_{50} values, where helicity is 50% of the maximum, are 5.5–5.7. Statistical analysis shows that these are not substantially different between POPC and POPS-containing bilayers. Thus, the decrease in pHD15 activity in POPS-containing bilayers is not due to differences in secondary structure.

Taken together, the data in Figs. 2 and 3 show that binding and secondary structure are very similar in vesicles made

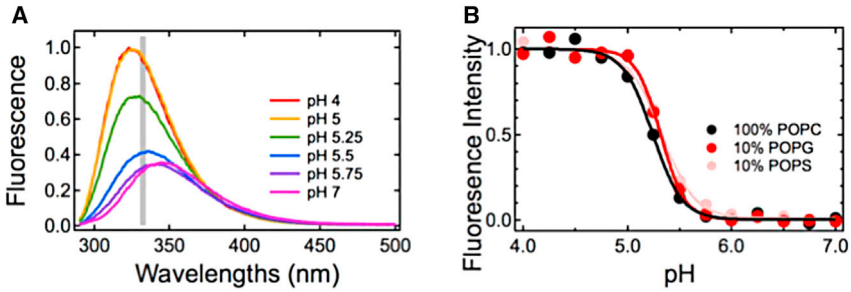

FIGURE 2 Binding of pHD15 to vesicles composed of POPC, 10% POPG, and 10% POPS membranes as measured by tryptophan fluorescence. (*A*) Tryptophan fluorescence spectra measured after a 1-h incubation of peptide with 10% POPG membranes at P:L = 1:50. (*B*) The fluorescence from 330 to 335 nm, as indicated by the gray region in (*A*), was averaged, normalized, and plotted as a function of pH. To see this figure in color, go online.

from 100% POPC or POPC + 10% POPS. To explain lower activity in POPS-containing bilayers, we hypothesize that the headgroups influence insertion of the peptide from an interfacially bound state into the transmembrane pore state. To explore other factors that may regulate insertion, we next assessed the macromolecular poration activity of pHD15 in PC bilayers of varying thickness.

Macromolecular leakage across membranes of varying thickness

The unusual pore-forming activity of the pHD peptides is due to their ability to insert into a membrane-spanning orientation and stabilize the circumference of a very large pore (10). This would occur by having the hydrophobic surfaces of the amphipathic helices interact with the lipid hydrocarbon to reduce the cost of its exposure to water. As such, we hypothesize that a match between the length of the peptide helix and the thickness of the bilayer hydrocarbon will be important for function and that the thickness of a lipid bilayer will strongly influence the ability of pHD15 to form macromolecule-sized pores. To test this idea, we measured macromolecular poration as a function of pH and P:L in bilayers made from PC lipids with two identical monounsaturated acyl chains ranging from C14 to C20 (see Materials and methods). A few experiments were done in C22PC lipids that behaved the same as C20PC. The results, in Fig. 4, show a remarkable sensitivity of macromolecular poration activity to bilayer thickness. In the thinnest bilayer, C14PC, the activity of pHD15 is similar to, or even higher than, its activity in POPC bilayers (C16:0,C18:1(9)PC), shown in the dashed red line. In bilayers made from C16PC and dC18PC, the activity of pHD15 is significantly reduced, and pH_{50} values are shifted to a lower pH. In bilayers made from C20PC lipids, poration activity is not detectable at any *P:L*; thus, LIC_{50} >> 1:50. Similarly, no leakage was observed in C22PC bilayers, even at high P:L and low pH (data not shown). The entire pH and concentration series of experiments were not performed in C22PC lipids because there was no activity at the highest peptide concentration and low pH.

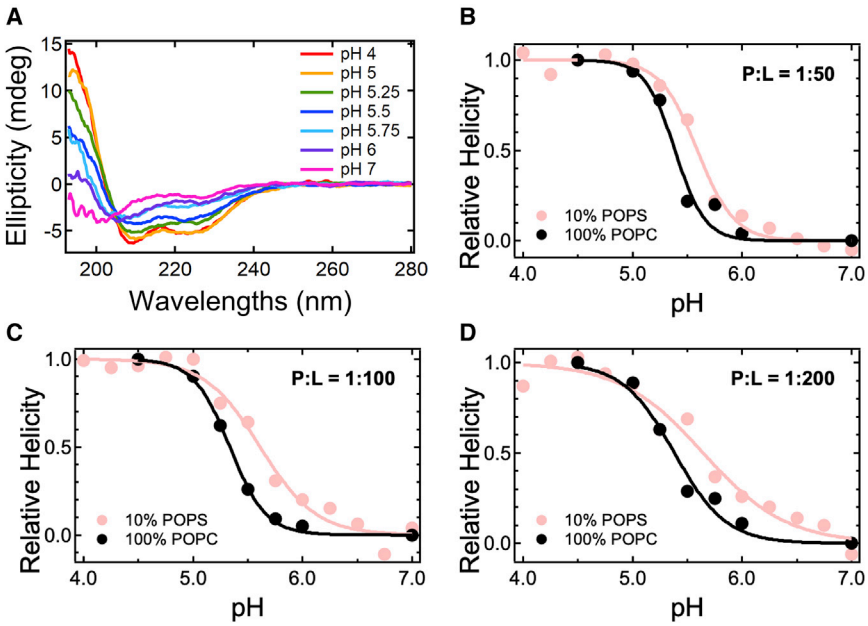

FIGURE 3 Folding of pHD15 in 10% POPS membranes. pHD15 was incubated with 10% POPS membranes for 1 h before the CD spectra were measured. (*A*) An example set of CD spectra at P:L = 1:100. (*B–D*) The helicity was calculated from the average 217–227 nm ellipticity and normalized between 0 and 1. Results for POPC and POPC with 10% POPS are compared for three different peptide concentrations: P:L 1:50 (*B*), 1:100 (*C*), and 1:200 (*D*). The difference between helicity curves in the two lipid bilayers is not statistically significant. *p*-values are 0.299 (*B*), 0.101 (*C*), and 0.053 (*D*). To see this figure in color, go online.

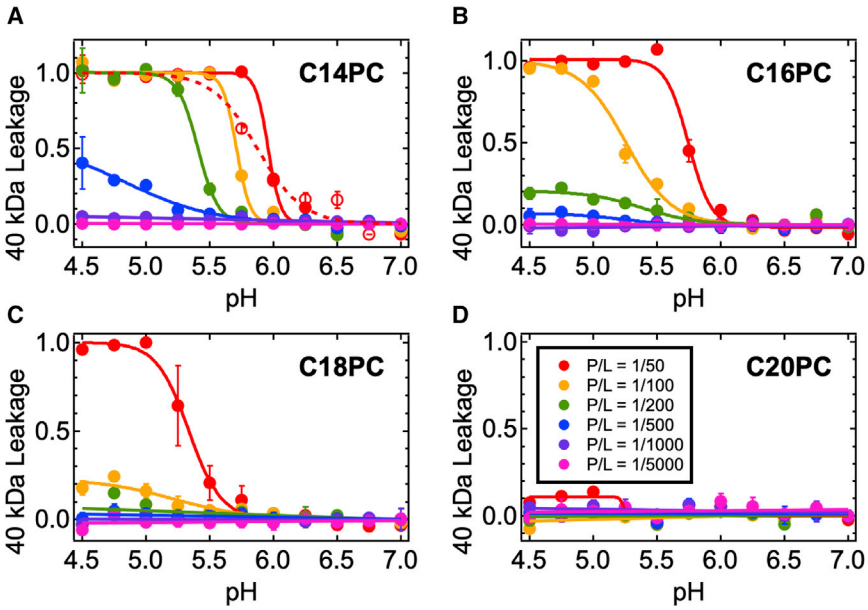

FIGURE 4 Macromolecular leakage across membranes of increasing thickness in response to pHD15. pHD15 was incubated for 1 h at room temperature with 1 mM lipids before leakage was measured. This experiment was performed with membranes composed of PC headgroup lipids with singly unsaturated acyl chains with 14 (*A*), 16 (*B*), 18 (*C*), and 20 carbons (*D*). For comparison, the activity of pHD15 in POPC membranes is shown as a dashed red line in (*A*). The errors bars represent standard deviations. To see this figure in color, go online.

As we did for anionic bilayers above, we measured the binding of pHD15 to PC bilayers of different thicknesses (Fig. 5). Binding was measured by fluorescence titration (35) as a function of pH at several fixed P:L ratios. Under all conditions, pHD15 binds to all bilayers in a pH-dependent manner. Essentially, no peptide is bound to any membrane at pH 7, but ~100% of the peptide is bound at pH $\leq$ 5 to all membranes, including the long chain PC bilayers where we observe no macromolecular poration activity. Thus, the lack of activity in C20PC bilayers is not due to a lack of membrane-bound peptide.

Throughout this work, we model binding as a partitioning process (52), and thus, we quantify binding through the fraction of peptide bound. Under ideal, infinite dilution conditions, the fraction of peptide bound at a fixed lipid concentration and pH will be independent of peptide concentration. If peptide concentration influences partitioning at a fixed lipid concentration, then the behavior of the system is cooperative. The dependence of pH_{50} on peptide concentration, which we express as P:L because lipid concentration is fixed, is a measure of cooperativity. Under ideal conditions, peptide concentration will not influence binding, and thus, pH_{50} will not depend on peptide concentration. Negative cooperativity will lead to a decrease in pH_{50} with increasing P:L, whereas positive cooperativity will lead to an increase in pH_{50} with increasing P:L. To further illustrate cooperativity, in Fig. 5 *F*, we plot pHD15 binding to C14PC, C18PC, and C22PC lipids. All data are for pH 5 and 1 mM lipid and are plotted versus peptide concentration. This plot shows positive cooperativity in C14PC bilayers, noncooperativity in C18PC bilayers, and negative cooperativity in C22PC bilayers.

The literature contains many examples of negative cooperativity, mostly because of electrostatic repulsion or loss of electrostatic attraction, caused by accumulation of charged peptide on the bilayer (53). Positive cooperativity, which can indicate self-assembly of peptides in the membrane, is much less common, but it has been reported (54). Interestingly, both behaviors can be seen, for the same peptide, in the binding data in Fig. 5, *F–H*. To the best of our knowledge, this is the first example of such complex behavior. Binding of pHD15 to the thinnest bilayer displays distinct positive cooperativity; binding increases and pH_{50} increases by ~0.8 pH units between P:L 1:1000 and P:L 1:50. As bilayer thickness increases, cooperativity changes to negative. There is little or no cooperativity in C16PC bilayers and slight negative cooperativity in C18PC bilayers, where pH_{50} decreases 0.3 units between P:L 1:1000 and P:L 1:50. In the thickest C20PC bilayers, negative cooperativity is the highest; pH_{50} decreases by 0.8 units between P:L 1:50 and P:L 1:1000. The change in pH_{50} values as a function of P:L is summarized in Fig. 5 *G*. The slopes of these curves are plotted in Fig. 5 *H*.

In Fig. 6, we use the measured binding to plot macromolecular poration activity as a function of peptide bound per vesicle (P_{bound}:Vesicle). This plot shows the inherent activity of membrane-bound peptide. Previously, we showed that all activity measurements in POPC, at different peptide concentrations and different pH values, fell on a single curve, meaning that the primary determinant of activity was the peptide bound per vesicle (calculated assuming a 100-nm diameter vesicle and an area per lipid of 70 $Å^2$, which yields ~100,000 lipids per vesicle) (10). Here in Fig. 6 *A*, this is not the case; there are differences in the inherent activity of bound peptide. In the presence of 10% PS, the curve shifts rightward, demonstrating a decrease in the inherent activity compared to 100% POPC. However, this change is small

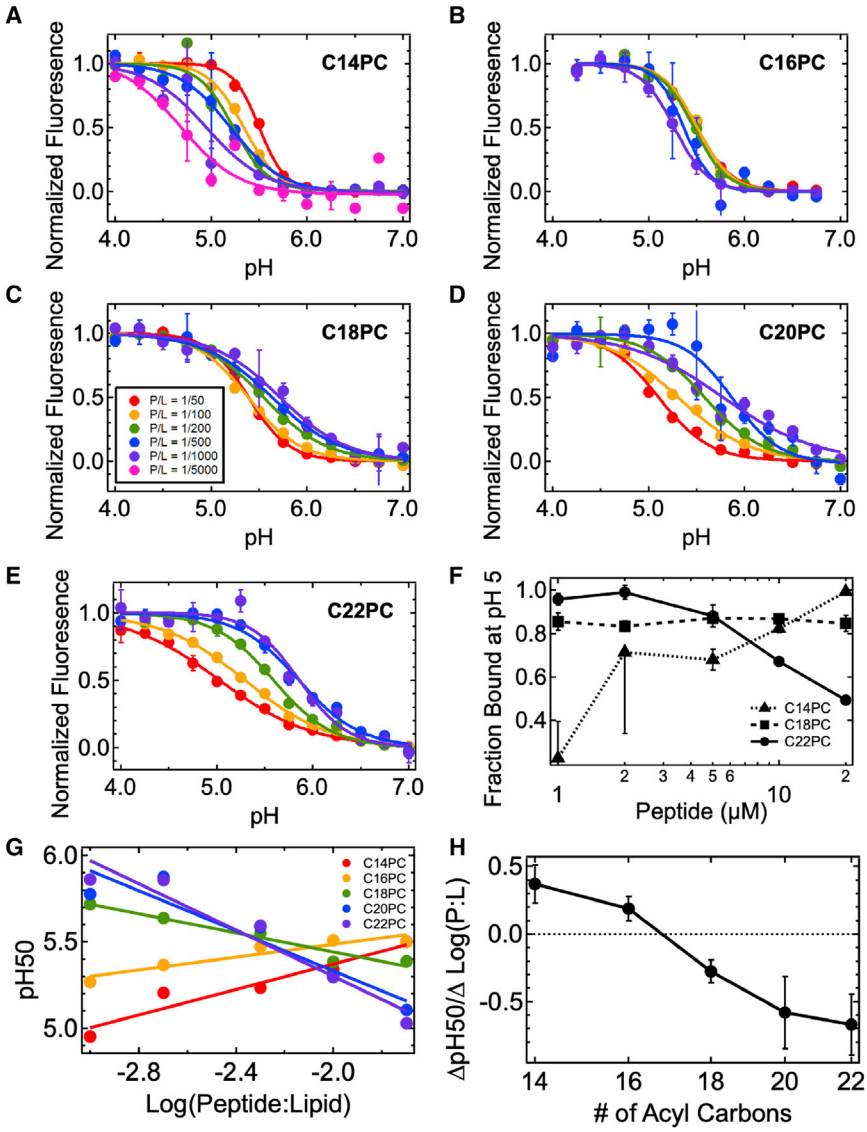

FIGURE 5 Binding of pHD15 to increasingly thicker membranes, as monitored by tryptophan fluorescence. (*A–E*) Binding of pHD15 to vesicles composed of singly unsaturated acyl chains of 14 (*A*), 16 (*B*), 18 (*C*), 20 (*D*), and 22 (*E*) carbons was measured after 1-h incubation with 1 mM lipids at a P:L of 1:50 to 1:5000. The fluorescence at 330–335 nm was averaged and normalized. Data shown are the average of three samples. Error bars represent standard deviations. (*F*) Shown are binding data at pH 5 from (*A*, *C*, and *E*) plotted against peptide concentration. Lipid concentration is 1 mM for all measurements. Data for C14PC show positive cooperativity, whereas data for C22PC show negative cooperativity. (*G*) Shown is the change in pH_{50} of binding curves, acquired for pHD15 binding to membranes of various thicknesses. The pH_{50} is plotted as a function of acyl chain carbons. (*H*) Shown are the slopes of the pH_{50} in (*F*), plotted as a function of P:L. The pH_{50} values were calculated by a sigmoidal fit of the tryptophan fluorescence versus pH curves shown in (*A*)–(*E*). To see this figure in color, go online.

compared to the remarkable change in activity with bilayer thickness (Fig. 6 *B*). The midpoint of the leakage curve shifts from an extraordinary potency at ~100 peptides per vesicle (LIC_{50} ~1:1000) in C14PC bilayers to essentially no measurable activity >>2000 peptides:vesicle or P:L >> 1:50 in C20PC or thicker bilayers.

Orientation of pHD15 in membranes of increasing thickness

For the pHD peptides, we have hypothesized that the formation of large pores is enabled by peptides that are oriented perpendicular to the plane of the bilayer (10). To determine the propensity for transmembrane orientation of the peptide in thin and thick membranes, we collected oriented circular dichroism (OCD) spectra (55–58) of oriented multibilayer samples of C14PC- and C22PC-containing pHD15 at P:L = 1:50. Spectra were collected in dry bilayers, which strongly disfavor helix insertion (57), and bilayers hydrated through the vapor phase either with pure water or with water containing 2% (v/v) acetic acid. In both C14PC and C22PC membranes, the dry spectra have two minima, at 212 and 222 nm (Fig. 7). The spectral shapes are similar to each other and are consistent with an α-helical peptide that is oriented predominantly parallel to the membrane surface (59). After hydration with water through the vapor phase, the shape of the C14PC spectrum shifts such that the intensity of the 212-nm peak decreases (Fig. 7 *A*). These changes suggest a transition toward a transmembrane state. Indeed, if the hydrated spectrum is assumed to be a linear combination of the dry spectrum and the spectrum of a helical peptide in a transmembrane orientation (59–61), the water-hydrated spectrum corresponds to ~20% of the peptides in the transmembrane orientation (Fig. 7 *B*). In C22PC membranes, the

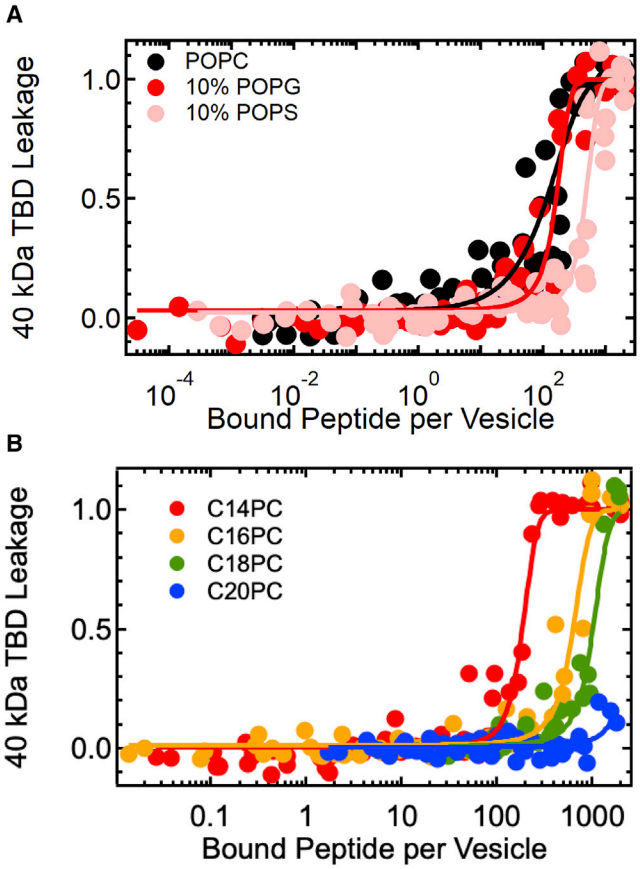

FIGURE 6 Activity versus bound peptide per vesicle for various lipid compositions. We estimate 100,000 lipids per vesicle (see text). The leakage is shown for POPC, 10% POPS, and 10% POPG vesicles (*A*) and in membranes of various thicknesses (*B*). To see this figure in color, go online.

OCD spectra do not change at all when hydrated with pure water (shown in Fig. 7 *C*), indicating that no insertion takes place. Although it is difficult to know the effective pH of these multibilayer samples, we also hydrated the bilayers with water containing 2% acetic acid. In C14PC bilayers, hydration with 2% acetic acid causes the same change as hydration with pure water, but to a much greater degree (Fig. 7 *D*), supporting our conclusion that the spectral change is due to membrane insertion. On the other hand, hydration of pHD15 in C22PC bilayers with 2% acetic acid did not cause any change in the shape of the OCD spectra, indicating again that the peptide remains oriented parallel to the surface of the membrane. The observed insertion of pHD15 in C14PC bilayers and the lack of insertion in C22PC bilayers is consistent with the observed poration activities.

Molecular dynamics simulations of pHD15 transmembrane configurations

To explore the possible geometries of pHD15 inserted into bilayers, we performed fully atomistic molecular dynamics simulations in a periodic bilayer containing one fully protonated pHD15 peptide, starting in a transmembrane α-helix state, and ~280 hydrated lipid molecules. Simulations were run in three lipids: 1) C14PC and 2) POPC, in which pHD15 is active, and 3) C20PC, in which pHD15 is not active. The simulations were not meant to understand the architecture of the macromolecule-sized pore induced by the peptide. This would be a difficult undertaking, given the large size of the pores and the lack of any detailed ultrastructural information (10). Instead, the goal of these simulations was to develop structural hypotheses by exploring the geometry of pHD15 inserted into PC bilayers of varying thicknesses. We were especially interested in the match/mismatch between the hydrophobic thickness of the bilayers and the hydrophobic face of the peptide.

For the length of the simulations (~350 ns each), the protonated peptide remained inserted in a membrane-spanning configuration, and the bilayer remained stable. We note that the translocation of the peptide termini is expected to be much slower than the timescale of these simulations, and therefore, the inserted state may be metastable. Transmembrane pHD15 was helical throughout the simulations except for a few residues on each termini (Fig. 8 *A*) and around the helix-breaking proline 14, consistent with experimental measurements (10). The pHD15 peptide maintained its distinct bend in the region of Pro14. This is a well-known and critical structural feature of the parent peptide melittin and is a feature that was also strongly selected for in the screen that led to the peptide MelP5 (61) used as a template to discover the pHD peptides. The bent helix is highly amphipathic, with a continuous hydrophobic surface on one side and a continuous polar/charged surface on the other, comprised of the six acidic residues and two histidines, shown in Fig. 8 *B*.

In Fig. 8 *C*, we show how the simulated peptide structures align with the interface and hydrocarbon core of the three simulated lipid bilayers. Only the lipid phosphate and carbonyl groups are shown (in *red* and *orange*, respectively) to delineate the boundaries of the interfacial regions. In particular, the carbonyls define the outer edge of the hydrocarbon core and inner edge of the interfacial zone. The empty space in between corresponds to mostly hydrocarbon (62), which is not shown for clarity. Some individual amino acid side chains are shown in spacefilling mode to provide reference points. In particular, the ends of the nonpolar face of the helical N- and C-terminal helical segments are shown by green spacefilling display of side chains Val5 and Leu6 on the N-terminus and Ala22 and Ala23 on the C-terminus. The polar face is marked by His7 and His21 in blue. For reference, Pro14 and Trp19 are also shown.

The transbilayer distributions of some of the lipid and peptide groups highlighted in the snapshots are shown in Fig. 8, *D–F*. These distributions, which are from the last 100 ns of each simulation, are unimodal and roughly Gaussian, except for the peptide in C20PC lipids (Fig. 8 *F*), which has a

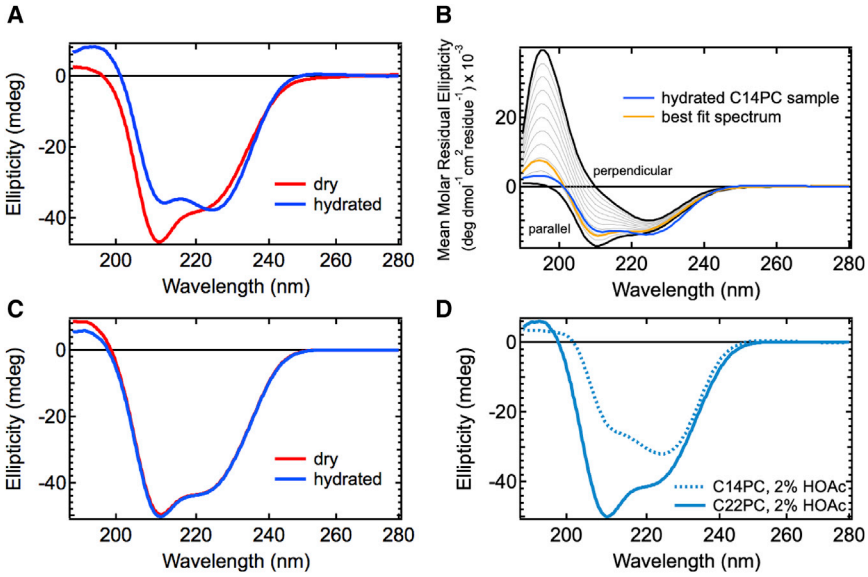

FIGURE 7 OCD spectra of pHD15 in membranes of different thickness. (*A*) Shown is a comparison of the OCD spectra of pHD15 in stacked, oriented bilayers composed of C14PC lipids on a quartz substrate in the dry state and after 70 min of hydration with pure water through the vapor phase. The average of eight spectra measured at 45° rotations of the sample around the beam axis is shown. The lipid-only spectra have been subtracted. (*B*) The OCD spectrum of pHD15 in hydrated C14PC membrane is shown in blue, and theoretical OCD spectra for helices that are parallel or perpendicular to the membrane plane are shown in black. Linear combinations of these basis spectra, in increments of 10% increase in perpendicular orientation, are shown in gray. The best fit spectrum, representing ~20% perpendicular helix, is in orange. (*C*) Shown is a comparison of the OCD spectra of pHD15 in stacked, oriented bilayers composed of C22PC lipids on a quartz substrate in the dry state and after 70 min of hydration with pure water through the vapor phase. (*D*) Shown are OCD spectra of pHD15 in C14PC and C22PC lipids, hydrated with water containing 2% glacial acetic acid. To see this figure in color, go online.

distinctly bimodal distribution, indicating the existence of two insertion locations along the bilayer normal. The horizontal bars in these panels show how the distributions of the outermost hydrophobes, Val5 and Ala23, align with the inner edge of the bilayer interface. In all simulations, the distance between Val5 and Ala23 is very similar (mean = 25.5 ± 0.5 Å), and thus, the bends around Pro14 are also very similar (data not shown). The vertical arrows show that the distance spanned by the hydrophobic amino acid residues along the bilayer normal increases from around 15 Å in C14PC to 23 Å in C20PC, indicative of a decreasing overall tilt of the peptide axis in the bilayer as the bilayers get thicker.

The simulations suggest a hydrophobic thickness mismatch between the peptide and the C20PC bilayer but not in the case of C14PC and POPC bilayers. This can be seen in the transbilayer profiles in Fig. 8. In C14PC and POPC bilayers, Val5 and Ala23 are simultaneously in contact with the two bilayer carbonyl distributions and the peptide resides at a stable insertion depth in these bilayers as shown by the unimodal number density distributions. On the other hand, in C20PC bilayers, the peptide shows a distinct bimodal number density distribution. The peptide exists in two insertion depths, one shifted toward the C-terminus and one shifted toward the N-terminus. We speculate that in neither of these states do the terminal hydrophobic groups make sufficient contact with both interfaces simultaneously. Therefore, the data and the simulations reveal hydrophobic matching as a critically important factor for pHD15 activity. Similarly, we show that the overall tilt angle of pHD15 is highest in C14PC and is nearly zero in C20PC bilayers, suggesting the possibility that tilt angle may also be important for macromolecular poration.

DISCUSSION

Membrane binding

To assemble into nm-sized pores in membranes at an acidic pH, the synthetically evolved pore-forming peptide pHD15, and other members of the same family (10), must bind spontaneously to lipid bilayers in a pH-dependent manner. As the pH decreases, the fraction of peptide bound increases with a sharp sigmoidal dependence. Midpoints of binding, which we call pH_{50}, range from pH 5 to pH 6 for pHD15, depending on peptide concentration and lipid composition. pHD15 has nine protonatable groups: six acidic D/E residues and three basic groups with two basic histidines and the free N-terminus. Its predicted net charge at a neutral pH is ~−4, but at pH ≤ 6, where the peptide has activity, the histidines and acidic side chains are at least partially protonated, reducing the net charge perhaps to around neutral. The fact that binding at a low pH does not change when the bilayers contain 10% anionic lipids supports the idea that the peptides are close to neutral. Some other pHD peptides have lysines in the two basic positions, which remain fully protonated, instead of histidines that have pKa ~6.5. However, the pH dependencies of binding are similar for all peptides (10). Thus, we do not believe that basic-acidic side-chain interactions are critical for macromolecular poration. Instead, electrostatic repulsions between multiple acidic side chains with helical spacings at a neutral pH inhibit helix formation, which inhibits membrane binding. The partial protonation of

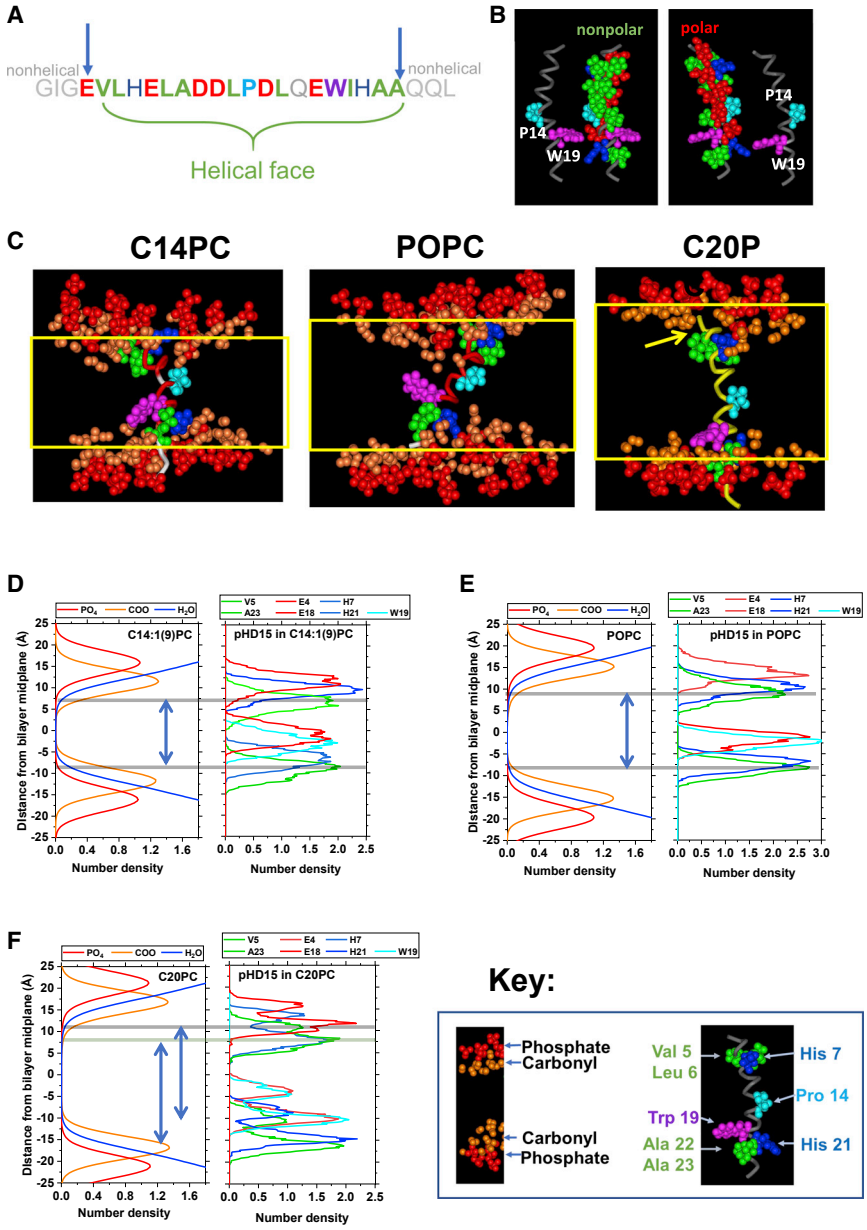

FIGURE 8 Molecular geometries of pHD15 and PC bilayers of different thicknesses. (*A*) Shown is the sequence of pHD15. Colored residues are consistently helical in the molecular dynamics simulations in all bilayers. Matching colors are used in the other panels. Hydrophobes are green, and acidic and basic residues are red and blue, respectively. Proline 14 is light blue, and tryptophan 19 is purple. See key at bottom. (*B*) The opposing polar and nonpolar faces of pHD15 are shown. The same structure is shown four times. On the left, we show backbone structure with Pro14 and Trp19 in spacefill, as well as the nonpolar (*green*) and polar (*red*) residues. In this orientation, the green nonpolar face is evident. On the right, the peptide is rotated 90° around the *y* axis, showing the acidic and basic face in red and blue, respectively. (*C*) Shown is a snapshot of equilibrated simulations. The lipid hydrocarbon has been removed, and the bilayer thickness is delineated by the phosphate and carbonyl groups in red and orange, respectively. See key. The ends of the pHD15 helix are shown by Val5, Leu6 (*green*), and His7 (*blue*) on the N-terminus and by His21, Ala22, and Ala23 on the C-terminus. For comparison, the structures have been aligned so that all peptides have a similar orientation. In C14PC and POPC bilayers, the helix ends, as defined above, are in contact with the two bilayer interfaces. In C20PC bilayers, the helix ends cannot contact the two interfacial regions at the same time. The yellow arrow shows the gap. (*D*–*F*) Shown are transbilayer distributions of lipid groups, water, and amino acids, derived from the molecular dynamics simulations. Number densities along the bilayer normal are shown for C14PC (*D*), POPC (*E*), and C20PC (*F*). Horizontal bars mark the maximum of the number density distributions of Val5 and Ala23, residues that are at the ends of the hydrophobic face of the helix. The colors used here match the highlighted molecular groups shown above. To see this figure in color, go online.

these groups with decreasing pH drives folding and binding by decreasing the cost of α-helix formation.

The effect of headgroup

In a recent publication, we showed that the effects of both pH and P:L on pHD peptide activity in POPC bilayers can be fully accounted for by their effects on the amount of peptide bound to each vesicle (10). If we express peptide concentration as P_{bound}:vesicle, then data collected at various pH and P:L values become coincident (10). Peptide bound per vesicle is the primary determinant of macromolecular poration activity in POPC. Thus, under all conditions, ~100 peptides bound to a POPC vesicle (P:L = 1:1000) are enough to cause macromolecular poration. In the experiments described here, we tested the hypothesis that binding is the only determinant of activity when POPC bilayers also contain 10% POPG or 10% POPS by plotting macromolecular poration as a function of P_{bound}:vesicle (Fig. 6 *A*). The curves are not coincident. Compared to 100% POPC, the inherent macromolecular poration activity of membrane-bound pHD15 in vesicles containing 10% POPS is decreased. The inclusion of 10% POPG has a smaller effect on activity. We showed that binding and structure are not strongly affected by POPG or POPS. Instead, the headgroup moieties of POPS must contribute negatively to insertion of

the peptide into the membrane-spanning configuration. The fact that POPG and POPS have different effects further indicates that the changes in activity cannot be explained by surface charge alone. PS is known to form interheadgroup hydrogen bonds (63), so it is possible that PS stabilizes the peptide in a surface-bound orientation, relative to the inserted pore state (64).

The effect of bilayer thickness on activity

The effect of bilayer thickness on macromolecular poration is dramatic. The activity of pHD15 in bilayers made from C14PC is similar to its highly potent activity in POPC. However, increasing the chain length by four carbons to C18PC causes a substantial decrease in activity and a downward shift in pH_{50}. When chain length is increased by six carbons to C20PC, macromolecular poration does not occur at any peptide concentration measured. The inherent pore-forming potency of pHD15 decreases by more than 100-fold in thicker bilayers compared to thin bilayers, despite the fact that the peptide binds similarly to all of these bilayers.

Interestingly, a very similar sharp decrease of peptide-induced permeabilization on increasing bilayer thickness has been reported previously (65). In this case, the authors studied the release of the small molecule carboxyfluorescein by the peptide δ-lysin using the same set of PC lipids that we use here. The release rate of carboxyfluorescein is at least 100-fold lower in C20PC compared to C14PC. Because δ-lysin, unlike pHD15, is a transient pore former (66) and does not insert across membranes to form equilibrium membrane-spanning pores, these authors hypothesized that the effect could be explained by changes in the bilayer bending modulus, a macroscopic bilayer property. As the pHD peptides self-assemble into pore structures comprised of membrane-spanning helices, we focus on microscopic properties, and we explain the effect of bilayer thickness on pHD15 activity mainly in terms of hydrophobic mismatch. However, we recognize that other bilayer properties likely also contribute to the overall activity.

Mechanistic hypothesis

For the peptide pHD15, membrane binding and folding into α-helical secondary structure are tightly coupled to each other and are only slightly dependent on membrane surface charge or bilayer thickness. Binding and folding are promoted by bilayer interfacial zones (58,67,68), without requiring insertion into a transmembrane state. We have previously speculated that the pHD peptides and the related macrolittins (60) exhibit their unique macromolecular poration activity at a low concentration because they are thermodynamically stable in a transmembrane state, thus stabilizing the circumference of large pores (10). Here, we show further evidence supporting the hypothesis that insertion of the pHD peptide from a surface bound to a transmembrane state is the critical step in macromolecular poration. Thus, the activity of the pHD peptides can be described with the four-step model of membrane protein folding (68,69). In the first and second steps, the unstructured peptide in solution partitions into the bilayer interface, driving the formation of α-helical secondary structure due to partitioning-folding coupling (68). In the third step, interfacially bound peptides insert across the bilayer, and in the fourth step, the inserted peptides self-assemble to form the macromolecule-sized pore.

The step that endows the pHD peptides with membrane selectivity is insertion of the peptide into the transmembrane orientation and perhaps also subsequent self-assembly into macromolecule-sized pores.

To better understand these phenomena, we used molecular dynamics simulations to explore the geometries of pHD15 in bilayers composed of C14PC, POPC, and C20PC. The goal of the simulations was to explore the potential geometries of lipids and peptides and to measure the match/mismatch between the hydrophobic surface of the peptide and the hydrocarbon core of the bilayers. We inserted a single pHD15 peptide, with its acidic and basic side chains protonated, in a membrane-spanning orientation in bilayers made from each of the three lipids and allowed the systems to equilibrate. Peptide transitions from membrane spanning to surface orientations are very unlikely to occur on these timescales, so the equilibrated structures are metastable. Yet examination of the lipids and transmembrane peptide structures can provide insights into the match, or mismatch, between the peptide hydrophobic face length and the bilayer thickness.

The simulations show a bend of the peptide α-helix at Pro14, a well-known and conserved feature of the parent peptide melittin (70) and of all peptides we have evolved from it (10,60,61). One surface of the kinked α-helix comprises a continuous hydrophobic face that will interact with the lipids in the pore structure. The other surface comprises the polar face, containing the six acidic residues and two histidines, that will likely create the water-exposed surface of the pore. Interestingly, the simulations show that the critical hydrophobic thickness of the peptide includes the alanine at the 23rd position. This may explain why replacement of Lys23 with Ala23 was one of the critical substitutions observed in the first generation of synthetic evolution of the very potent MelP5 from the parent melittin (66).

Based on the geometries obtained from these simulations, we speculate that the helical hydrophobic surfaces can interact with the bilayer hydrocarbon core and extend slightly into both lipid interfaces in C14PC and POPC bilayers. On the other hand, the hydrophobic face of pHD15 cannot simultaneously contact both interfaces in C20PC bilayers, despite the fact that the tilt angle decreases and the bend at Pro14 decreases. The insertion of pHD15 into C20PC bilayers is not optimal because it gives rise

to a hydrophobic mismatch between the peptide and the bilayer (17,71,72). It is also possible that the low tilt angle in C20PC is not compatible with macromolecular poration.

The evolution of membrane selectivity

We previously evolved the pHD peptides to have the unique property of pH-triggered self-assembly into very unusual nm-sized pores in PC bilayers (9). Here, we show that these peptides have 1) moderate selectivity for bilayers made from 100% PC over bilayers also containing PS and 2) very strong selectivity for thin bilayers over thick bilayers. We believe that engineering or optimizing membrane selectivity will be critical for further development of pore-forming peptides across the field. Our results suggest that pH-sensitive peptides can be engineered to be highly specific for specific membrane compositions. The optimization of such membrane-selective peptides can be accomplished using additional generations of synthetic molecular evolution just as we evolved MelP5 from melittin and evolved the pHD peptides from MelP5.

ACKNOWLEDGMENTS

Simulations were performed on HLRN, The North-German Supercomputing Cluster.

This work was funded by National Institutes of Health R01 GM111824 and National Science Foundation DMR 1710053 (W.C.W.) and National Science Foundation DMR 1709892 (K.H.). A.-N.B. was supported in part by funding from the European Union's Horizon 2020 research and innovation program under the Marie Sklodowska-Curie grant agreement No 860592, Innovative Training Network 'Proton and proton-coupled transport'.

REFERENCES

1. Guha, S., J. Ghimire, …, W. C. Wimley. 2019. Mechanistic landscape of membrane-permeabilizing peptides. *Chem. Rev.* 119:6040–6085.
2. Easton, D. M., A. Nijnik, …, R. E. W. Hancock. 2009. Potential of immunomodulatory host defense peptides as novel anti-infectives. *Trends Biotechnol.* 27:582–590.
3. Jenssen, H., P. Hamill, and R. E. W. Hancock. 2006. Peptide antimicrobial agents. *Clin. Microbiol. Rev.* 19:491–511.
4. Moulay, G., C. Leborgne, …, B. Bechinger. 2017. Histidine-rich designer peptides of the LAH4 family promote cell delivery of a multitude of cargo. *J. Pept. Sci.* 23:320–328.
5. Mäe, M., and U. Langel. 2006. Cell-penetrating peptides as vectors for peptide, protein and oligonucleotide delivery. *Curr. Opin. Pharmacol.* 6:509–514.
6. Komin, A., L. M. Russell, …, P. C. Searson. 2017. Peptide-based strategies for enhanced cell uptake, transcellular transport, and circulation: mechanisms and challenges. *Adv. Drug Deliv. Rev.* 110–111:52–64.
7. Nishimura, Y., K. Takeda, …, A. Kondo. 2014. A display of pH-sensitive fusogenic GALA peptide facilitates endosomal escape from a Bionanocapsule via an endocytic uptake pathway. *J. Nanobiotechnology.* 12:11.
8. Akishiba, M., T. Takeuchi, …, S. Futaki. 2017. Cytosolic antibody delivery by lipid-sensitive endosomolytic peptide. *Nat. Chem.* 9:751–761.
9. Wiedman, G., S. Y. Kim, …, K. Hristova. 2017. pH-Triggered, macromolecule-sized poration of lipid bilayers by synthetically evolved peptides. *J. Am. Chem. Soc.* 139:937–945.
10. Kim, S. Y., A. E. Pittman, …, K. Hristova. 2019. Mechanism of action of peptides that cause the pH-triggered macromolecular poration of lipid bilayers. *J. Am. Chem. Soc.* 141:6706–6718.
11. Dowhan, W. 1997. Molecular basis for membrane phospholipid diversity: why are there so many lipids? *Annu. Rev. Biochem.* 66:199–232.
12. Papahadjopoulos, D., and N. Miller. 1967. Phospholipid model membranes. I. Structural characteristics of hydrated liquid crystals. *Biochim. Biophys. Acta.* 135:624–638.
13. Shevchenko, A., and K. Simons. 2010. Lipidomics: coming to grips with lipid diversity. *Nat. Rev. Mol. Cell Biol.* 11:593–598.
14. Levental, I., and S. Veatch. 2016. The continuing mystery of lipid rafts. *J. Mol. Biol.* 428:4749–4764.
15. Lorent, J. H., K. R. Levental, …, I. Levental. 2020. Plasma membranes are asymmetric in lipid unsaturation, packing and protein shape. *Nat. Chem. Biol.* 16:644–652.
16. Barrera, F. N., J. Fendos, and D. M. Engelman. 2012. Membrane physical properties influence transmembrane helix formation. *Proc. Natl. Acad. Sci. USA.* 109:14422–14427.
17. Andersen, O. S., and R. E. Koeppe, II. 2007. Bilayer thickness and membrane protein function: an energetic perspective. *Annu. Rev. Biophys. Biomol. Struct.* 36:107–130.
18. Karabadzhak, A. G., D. Weerakkody, …, D. M. Engelman. 2018. Bilayer thickness and curvature influence binding and insertion of a pHLIP peptide. *Biophys. J.* 114:2107–2115.
19. Yu, X., and J. Zheng. 2012. Cholesterol promotes the interaction of Alzheimer β-amyloid monomer with lipid bilayer. *J. Mol. Biol.* 421:561–571.
20. Lee, D. K., A. Bhunia, …, A. Ramamoorthy. 2015. Detergent-type membrane fragmentation by MSI-78, MSI-367, MSI-594, and MSI-843 antimicrobial peptides and inhibition by cholesterol: a solid-state nuclear magnetic resonance study. *Biochemistry.* 54:1897–1907.
21. Teixeira, V., M. J. Feio, and M. Bastos. 2012. Role of lipids in the interaction of antimicrobial peptides with membranes. *Prog. Lipid Res.* 51:149–177.
22. Dowhan, W., and M. Bogdanov. 2009. Lipid-dependent membrane protein topogenesis. *Annu. Rev. Biochem.* 78:515–540.
23. Allende, D., S. A. Simon, and T. J. McIntosh. 2005. Melittin-induced bilayer leakage depends on lipid material properties: evidence for toroidal pores. *Biophys. J.* 88:1828–1837.
24. Babakhani, A., A. A. Gorfe, …, J. A. McCammon. 2008. Thermodynamics of peptide insertion and aggregation in a lipid bilayer. *J. Phys. Chem. B.* 112:10528–10534.
25. van Meer, G., D. R. Voelker, and G. W. Feigenson. 2008. Membrane lipids: where they are and how they behave. *Nat. Rev. Mol. Cell Biol.* 9:112–124.
26. Ziegler, A. 2008. Thermodynamic studies and binding mechanisms of cell-penetrating peptides with lipids and glycosaminoglycans. *Adv. Drug Deliv. Rev.* 60:580–597.
27. Lee, D. K., J. R. Brender, …, A. Ramamoorthy. 2013. Lipid composition-dependent membrane fragmentation and pore-forming mechanisms of membrane disruption by pexiganan (MSI-78). *Biochemistry.* 52:3254–3263.
28. Elmore, D. E. 2006. Molecular dynamics simulation of a phosphatidylglycerol membrane. *FEBS Lett.* 580:144–148.
29. Cornell, B. A., and F. Separovic. 1983. Membrane thickness and acyl chain length. *Biochim. Biophys. Acta.* 733:189–193.
30. Lee, T. H., M. A. Sani, …, M. I. Aguilar. 2018. Effect of phosphatidylcholine bilayer thickness and molecular order on the binding of the antimicrobial peptide maculatin 1.1. *Biochim. Biophys. Acta Biomembr.* 1860:300–309.
31. Phillips, R., T. Ursell, …, P. Sens. 2009. Emerging roles for lipids in shaping membrane-protein function. *Nature.* 459:379–385.

32. Wiedman, G., T. Fuselier, …, W. C. Wimley. 2014. Highly efficient macromolecule-sized poration of lipid bilayers by a synthetically evolved peptide. *J. Am. Chem. Soc.* 136:4724–4731.

33. Wiedman, G., W. C. Wimley, and K. Hristova. 2015. Testing the limits of rational design by engineering pH sensitivity into membrane-active peptides. *Biochim. Biophys. Acta.* 1848:951–957.

34. Stewart, J. C. 1980. Colorimetric determination of phospholipids with ammonium ferrothiocyanate. *Anal. Biochem.* 104:10–14.

35. Ladokhin, A. S., S. Jayasinghe, and S. H. White. 2000. How to measure and analyze tryptophan fluorescence in membranes properly, and why bother? *Anal. Biochem.* 285:235–245.

36. Kelley, L. A., S. Mezulis, …, M. J. E. Sternberg. 2015. The Phyre2 web portal for protein modeling, prediction and analysis. *Nat. Protoc.* 10:845–858.

37. Kelley, L. A., and M. J. E. Sternberg. 2009. Protein structure prediction on the Web: a case study using the Phyre server. *Nat. Protoc.* 4:363–371.

38. Humphrey, W., A. Dalke, and K. Schulten. 1996. VMD: visual molecular dynamics. *J. Mol. Graph.* 14:33–38, 27–28..

39. Brooks, B. R., R. E. Bruccoleri, …, M. Karplus. 1983. Charmm - a program for macromolecular energy, minimization, and dynamics calculations. *J. Comput. Chem.* 4:187–217.

40. Cheng, X., S. Jo, …, W. Im. 2013. CHARMM-GUI micelle builder for pure/mixed micelle and protein/micelle complex systems. *J. Chem. Inf. Model.* 53:2171–2180.

41. Mackerell, A. D., Jr., M. Feig, and C. L. Brooks, III. 2004. Extending the treatment of backbone energetics in protein force fields: limitations of gas-phase quantum mechanics in reproducing protein conformational distributions in molecular dynamics simulations. *J. Comput. Chem.* 25:1400–1415.

42. MacKerell, A. D., D. Bashford, …, M. Karplus. 1998. All-atom empirical potential for molecular modeling and dynamics studies of proteins. *J. Phys. Chem. B.* 102:3586–3616.

43. Foloppe, N., and A. D. MacKerell, Jr. 2000. All-atom empirical force field for nucleic acids: I. Parameter optimization based on small molecule and condensed phase macromolecular target data. *J. Comput. Chem.* 21:86–104.

44. Klauda, J. B., R. M. Venable, …, R. W. Pastor. 2010. Update of the CHARMM all-atom additive force field for lipids: validation on six lipid types. *J. Phys. Chem. B.* 114:7830–7843.

45. Jorgensen, W. L., J. Chandrasekhar, …, M. L. Klein. 1983. Comparison of simple potential functions for simulating liquid water. *J. Chem. Phys.* 79:926–935.

46. Kalé, L., R. Skeel, …, K. Schulten. 1999. NAMD2: greater scalability for parallel molecular dynamics. *J. Comput. Phys.* 151:283–312.

47. Phillips, J. C., R. Braun, …, K. Schulten. 2005. Scalable molecular dynamics with NAMD. *J. Comput. Chem.* 26:1781–1802.

48. Grubmuller, H., H. Heller, …, K. Schulten. 1991. Generalized Verlet algorithm for efficient molecular dynamics simulations with long-range interactions. *Mol. Simul.* 6:121–142.

49. Tuckerman, M., B. J. Berne, and G. J. Martyna. 1992. Reversible multiple time scale molecular-dynamics. *J. Chem. Phys.* 97:1990–2001.

50. Darden, T., D. York, and L. Pedersen. 1993. Particle mesh Ewald - an N.Log(N) method for Ewald sums in large systems. *J. Chem. Phys.* 98:10089–10092.

51. Essmann, U., L. Perera, …, L. G. Pedersen. 1995. A smooth particle mesh Ewald method. *J. Chem. Phys.* 103:8577–8593.

52. White, S. H., W. C. Wimley, …, K. Hristova. 1998. Protein folding in membranes: determining energetics of peptide-bilayer interactions. *Methods Enzymol.* 295:62–87.

53. Montich, G., S. Scarlata, …, J. Seelig. 1993. Thermodynamic characterization of the association of small basic peptides with membranes containing acidic lipids. *Biochim. Biophys. Acta.* 1146:17–24.

54. Wimley, W. C., K. Hristova, …, S. H. White. 1998. Folding of beta-sheet membrane proteins: a hydrophobic hexapeptide model. *J. Mol. Biol.* 277:1091–1110.

55. Olah, G. A., and H. W. Huang. 1988. Circular dichroism of oriented à helices. I. Proof of the exciton theory. *J. Chem. Phys.* 89:2531–2538.

56. Olah, G. A., and H. W. Huang. 1988. Circular dichroism of oriented à helices. II. Electric field oriented polypeptides. *J. Chem. Phys.* 89:6956–6962.

57. Harroun, T. A., W. T. Heller, …, H. W. Huang. 1999. States of natural melittin by oriented circular dichroism and neutron diffraction. *Biophys. J.* 76:A124.

58. Hristova, K., W. C. Wimley, …, S. H. White. 1999. An amphipathic alpha-helix at a membrane interface: a structural study using a novel X-ray diffraction method. *J. Mol. Biol.* 290:99–117.

59. Wu, Y., H. W. Huang, and G. A. Olah. 1990. Method of oriented circular dichroism. *Biophys. J.* 57:797–806.

60. Li, S., S. Y. Kim, …, K. Hristova. 2018. Potent macromolecule-sized poration of lipid bilayers by the macrolittins, a synthetically evolved family of pore-forming peptides. *J. Am. Chem. Soc.* 140:6441–6447.

61. Krauson, A. J., J. He, …, W. C. Wimley. 2013. Synthetic molecular evolution of pore-forming peptides by iterative combinatorial library screening. *ACS Chem. Biol.* 8:823–831.

62. Wiener, M. C., and S. H. White. 1992. Structure of a fluid dioleoylphosphatidylcholine bilayer determined by joint refinement of x-ray and neutron diffraction data. III. Complete structure. *Biophys. J.* 61:434–447.

63. Boggs, J. M. 1987. Lipid intermolecular hydrogen bonding: influence on structural organization and membrane function. *Biochim. Biophys. Acta.* 906:353–404.

64. Huang, H. W. 2000. Action of antimicrobial peptides: two-state model. *Biochemistry.* 39:8347–8352.

65. Pokorny, A., E. M. Kilelee, …, P. F. Almeida. 2008. The activity of the amphipathic peptide delta-lysin correlates with phospholipid acyl chain structure and bilayer elastic properties. *Biophys. J.* 95:4748–4755.

66. Wimley, W. C., and K. Hristova. 2019. The mechanism of membrane permeabilization by peptides: still an enigma. *Aust. J. Chem.* 73:96–103.

67. Hristova, K., C. E. Dempsey, and S. H. White. 2001. Structure, location, and lipid perturbations of melittin at the membrane interface. *Biophys. J.* 80:801–811.

68. White, S. H., and W. C. Wimley. 1999. Membrane protein folding and stability: physical principles. *Annu. Rev. Biophys. Biomol. Struct.* 28:319–365.

69. Engelman, D. M., Y. Chen, …, J. L. Popot. 2003. Membrane protein folding: beyond the two stage model. *FEBS Lett.* 555:122–125.

70. Terwilliger, T. C., and D. Eisenberg. 1982. The structure of melittin. II. Interpretation of the structure. *J. Biol. Chem.* 257:6016–6022.

71. Weiss, T. M., P. C. A. van der Wel, …, H. W. Huang. 2003. Hydrophobic mismatch between helices and lipid bilayers. *Biophys. J.* 84:379–385.

72. Petrache, H. I., D. M. Zuckerman, …, T. B. Woolf. 2002. Hydrophobic matching mechanism investigated by molecular dynamics simulations. *Langmuir.* 18:1340–1351.